PHYSICAL REVIEW B VOLUME 48, NUMBER 8 15 AUGUST 1993-II

Theory of the electronic structure of porous Si

Jian-Bai Xia* and Yia-Chung Chang
Department of Physics and Materials Research Laboratory, University of Illinois at Urbana-Champaign, 1110 West Green Street, Urbana, Illinois 61801
(Received 29 December 1992; revised manuscript received 18 March 1993)

A theoretical model for the electronic structure of porous Si is presented. Three geometries of porous Si (wire with square cross section, pore with square cross section, and pore with circular cross section) along both the [001] and [110] directions are considered. It is found that the confinement geometry affects decisively the ordering of conduction-band states. Due to the quantum confinement effect, there is a mixing between the bulk X and Γ states, resulting in finite optical transition matrix elements, but smaller than the usual direct transition matrix elements by a factor of 10^{-3}. We found that the strengths of optical transitions are sensitive to the geometry of the structure. For (001) porous Si the structure with circular pores has much stronger optical transitions compared to the other two structures and it may play an important role in the observed luminescence. For this structure the energy difference between the direct and the indirect conduction-band minima is very small. Thus it is possible to observe photoluminescence from the indirect minimum at room temperature. For (110) porous Si of similar size of cross section the energy gap is smaller than that of (001) porous Si. The optical transitions for all three structures of (110) porous Si tend to be much stronger along the axis than perpendicular to the axis.

I. INTRODUCTION

Recent observation of visible luminescence in porous Si at room temperature[1] has stimulated a great deal of interest in studying the origin of photoluminescence in porous Si. Bulk Si has an indirect band gap, which under normal circumstances prevents efficient interband radiative recombination. If the optical properties of Si become as useful as the electronic properties, the popular semiconductor would play as large a role in the emerging technology of optoelectronics as it has in the microelectronics revolution. Thus the understanding of the optical properties of porous Si is important from both the scientific and technological points of view. Many experimental and theoretical investigations have been devoted to this goal, and several conjectures of the origin of this visible-light emission have been proposed.

(1) The quantum-size confinement effect,[1-3] for which there is yet a lack of direct and decisive evidence. A correlation of Raman and photoluminescence spectra[4] showed that the origin of the luminescence is due to the quantum confinement of a microstructure having a characteristic dimension of 20–30 Å. Sanders and Chang[5] studied theoretically the electronic and optical properties of freestanding Si quantum wires with a square cross section. They found that for narrow quantum wires with widths around 8 Å, the average exciton oscillator strength is comparable to that of bulk GaAs. However, the average exciton oscillator strength decreases dramatically (faster than $1/L^5$) as the quantum-wire width L increases. First-principle calculations on similar structures lead to essentially the same conclusion.[6]

(2) Transition between band-tail states of hydrogenated amorphous Si due to the intrinsic disorder. A light emission at about 1.4 eV with an emission width of about 0.3 eV has been reported.[7] The x-ray photoelectron spectroscopy measurements of Si $2p$ and valence-band states in porous Si and crystalline Si (Ref. 8) demonstrated that the near-surface region of high porosity films exhibits visible luminescence consisting of amorphous Si.

(3) Phonon-assisted indirect transitions. The anomalous temperature dependences of the emission energy and emission intensity are attributed to the phonon participation.[9]

(4) Siloxene derivate present in porous Si. Brandt *et al.*[10] compared luminescence and vibrational properties of porous Si and chemically synthesized siloxene ($Si_6O_3H_6$) and its derivate. Based on the quantitative agreement of these two types of materials they attributed the strong room-temperature luminescence in porous Si to a siloxene derivate present in porous Si.

In this paper we present a theoretical model for studying the electronic structure of porous Si with wire as well as pore structures. We believe that in porous Si, both types of structures exist. The theoretical model combines the empirical pseudopotential method[11,12] with the degenerate perturbation method.[13,14] With this model we studied the quantum confinement effect of the porous Si in three different geometries, including a wire structure with a square cross section (square wire), a pore structure with a square cross section (square pore), and a pore structure with a circular cross section (circular pore). We found that the pore structure with a circular cross section has the strongest optical transition matrix element and it should play an important role in the luminescence

 ©1993 The American Physical Society

observed in porous Si. In Sec. II we introduce briefly the theoretical method, and in Sec. III we discuss the electronic states and optical transition matrix elements in porous Si with various cross sections and crystalline orientations.

II. THEORETICAL METHOD FOR POROUS SI

The cross sections of three different geometries of porous (001) Si are shown in Fig. 1, in which (a), (b), and (c) correspond to structures with square free-standing wires, square pores, and circular pores, respectively. In our super-cell model, the system has translational symmetries in the [001], [110], and [$\bar{1}$10] directions with periods a, $\frac{l\sqrt{2}}{2}a$, and $\frac{m\sqrt{2}}{2}a$, where l and m are integers which determine the size of the super cell. Because of the periodic structure of the model system, the wave function of the porous Si can be written in terms of Si bulk states with wave vectors $\mathbf{k}+\mathbf{g}(-\frac{\pi}{a}<k_z<\frac{\pi}{a})$, where $\mathbf{g}$ are reciprocal-lattice vectors of the model system enclosed within the first Brillouin zone of bulk Si. Here for bulk Si, we use the double unit cell as shown in Fig. 2(a) instead of the usual unit cell used for the diamond structure in order to satisfy the periodicity of porous Si. The corresponding Brillouin zone is shown in Fig. 2(b), which can be viewed as a folding of the usual Brillouin zone for the diamond structure. The states at the Γ point [$\mathbf{k}$=(0,0,0)] now comprise states at the Γ [$\mathbf{k}$=(0,0,0)] and X [$\mathbf{k}=(0,0,\frac{2\pi}{a})$] points in the usual Brillouin zone. The components of $\mathbf{g}$ along the [110] and [$\bar{1}$10] directions are given by

$$g_1=\frac{2\pi}{l\frac{\sqrt{2}}{2}a}l_1,\qquad l_1=-[(l-1)/2],\ldots,0,\ldots,[l/2], \tag{1}$$

$$g_2=\frac{2\pi}{m\frac{\sqrt{2}}{2}a}l_2,\qquad l_2=-[(m-1)/2],\ldots,0,\ldots,[m/2], \tag{2}$$

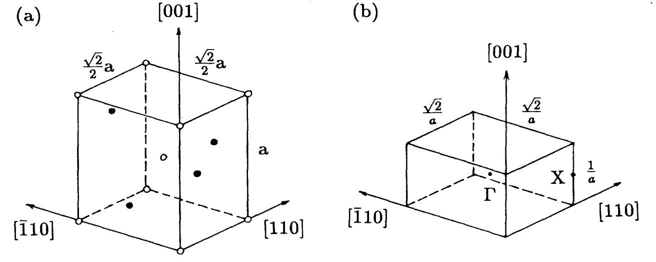

FIG. 2. Schemetic plots of (a) a unit cell and (b) the Brillouin zone used in the paper.

where we have used the symbol $[x]$ to denote an integer closest to and no larger than x. Using these bulk states as basis functions for the expansion of the wave functions for porous Si, we have

$$\Psi(\mathbf{r})=\sum_{n,\mathbf{g}}C_{n,\mathbf{k}+\mathbf{g}}\psi_{n,\mathbf{k}+\mathbf{g}}(\mathbf{r}), \tag{3}$$

where $\psi_{n,\mathbf{k}+\mathbf{g}}$ denotes the bulk Bloch states associated with the nth band and wave vector $\mathbf{k}+\mathbf{g}$.

For porous Si, the perturbation potential is caused by the open area in Fig. 1. We write

$$\Delta V(\mathbf{r})=\begin{cases}V_0 & \text{in the open area}\\ 0 & \text{in the filled area,}\end{cases} \tag{4}$$

where V_0 is large relative to the energy range considered. It is positive for the conduction-band states and negative for the valence-band states. Namely, the vacuum regions are replaced by bulk Si with the conduction bands rigidly shifted upward by a constant and the valence bands shifted downward by another constant. The problem now resembles that of a homojunction. The mixing of conduction-band states and valence-band states is neglected by solving the problem separately for conduction and valence bands. This is a valid procedure when the energy shifts due to the quantum confinement is small compared to the corresponding energy difference between the conduction- and valence-band states. We found this is satisfied for the size of the super cells considered. The magnitude of V_0 is adjusted by comparing

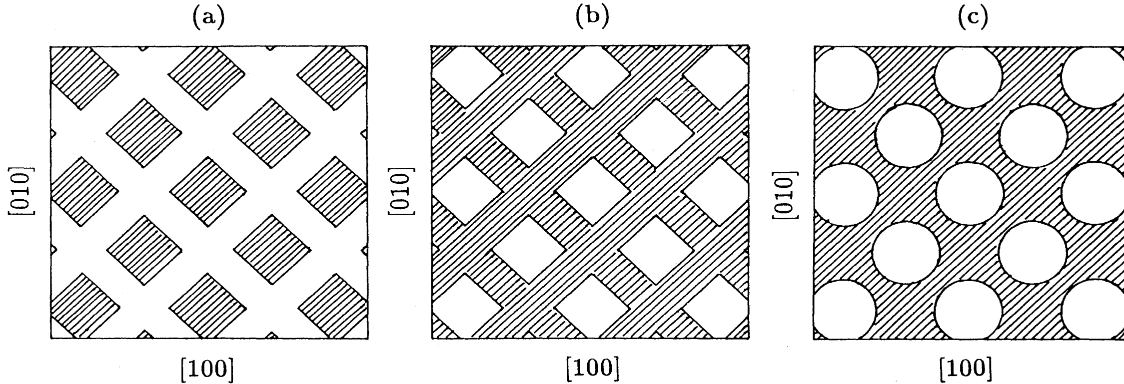

FIG. 1. Schemetic plots of the cross sections of porous (001) Si: (a) square standing wires, (b) connected structure with square pores, (c) connected structure with circular pores.

our results with the tight-binding results for the free-standing wires.[5] We found that the appropriate values for V_0 are 5.3 and 2.4 eV for the conduction- and valence-band states, respectively.

Using degenerate perturbation theory, we obtain a secular equation for porous Si,

$$|E_{n\mathbf{k}+\mathbf{g}}\delta_{nn'}\delta_{\mathbf{g}\mathbf{g}'} + \langle n\mathbf{k}+\mathbf{g}|\Delta V|n'\mathbf{k}+\mathbf{g}'\rangle - E| = 0, \quad (5)$$

where $E_{n,\mathbf{k}}$ is the energy eigenvalues of bulk Si. Because $\psi_{n\mathbf{k}}$ are composed of plane waves, the matrix elements of perturbation potential can be calculated easily; for example, in the circular pore structure [Fig. 1(c)],

$$\frac{1}{L^2}\int d\mathbf{r}\,\Delta V e^{i\mathbf{q}\cdot\mathbf{r}} = \frac{\pi R^2}{L^2}\frac{2J_1(qR)}{qR}V_0\delta_{q_z,0}, \quad (6)$$

where $J_1(x)$ is the Bessel function of first order, q is the magnitude of the vector $\mathbf{q} = \mathbf{g} - \mathbf{g}' + \mathbf{G} - \mathbf{G}'$ ($\mathbf{G},\mathbf{G}'$ are bulk reciprocal-lattice vectors), R is the radius of the circle, and L^2 is the area of the unit cell in the XY plane. Note that the matrix element vanishes unless $\mathbf{q}$ lies in the XY plane. When Δg approaches zero, it approaches $V_0\pi R^2/L^2$.

The form factors of the empirical pseudopotential for Si, $V(3)$, $V(8)$, $V(11)$ are not enough for the double unit-cell case, so we refer to the fitting formula of the form factor for Si,[15] but cut off at $q = \sqrt{11}(\frac{2\pi}{a})$. The number of plane waves used in the calculation is 123.

III. RESULTS

We calculated the electronic states and optical transition matrix elements

$$Q^i_{nn'} = \frac{2}{m_0}|\langle n|p_i|n'\rangle|^2, \qquad i = x,y,z \quad (7)$$

for the three geometries shown in Fig. 1. First we discuss the case of (001) porous Si. We choose the size of the unit cell to be $l = m = 10$ [see Eqs. (1) and (2)]. The length of each edge is $L = 10\frac{\sqrt{2}}{2}a = 38.4$ Å. In the first case, the length of each edge for the free-standing wire is taken as $6\frac{\sqrt{2}}{2}a = 23$ Å; in the second case, the length of each edge for the square pore is taken as $8\frac{\sqrt{2}}{2}a = 30.7$ Å; and in the third case, the radius of the circular pore is taken as $3.3a = 17.9$ Å.

The eigenenergies of the lowest four conduction-band states and the highest four valence-band states at Γ point [$\mathbf{k}$=(0,0,0)] for the three structures of (001) porous Si are shown in Table I. The lower-lying conduction-band states can be classified into two kinds: one consists of four nearly degenerate states, the other consists of two degenerate states. For the wire structure with a square cross section (case 1) the fourfold states are lowest, which is in agreement with the results of Sanders and Chang [Fig. 4(c) of Ref. 5]. However, for the pore structure with the square cross section the twofold states are lowest.

Figure 3 shows the band structure of the square-wire structure for the wave vector along the z direction. Comparing this figure with Fig. 3(c) of Ref. 5, we find that the band structure obtained here is quite similar to the tight-binding results in Ref. 5. In particular, the lowest-lying conduction bands are nearly fourfold degenerate with the twofold degenerate bands lying at approximately 0.2 eV above at the zone center. From the wave functions of these states it is found that the nearly fourfold degenerate bands are composed of bulk states with $\mathbf{k}$ near four conduction-band minima in the XY plane, $(\pm0.85,0,0)\frac{2\pi}{a}$, $(0,\pm0.85,0)\frac{2\pi}{a}$, and the twofold degenerate band is composed of bulk states with $\mathbf{k}$ near $(0,0,\pm0.85)\frac{2\pi}{a}$ in the z direction. Because the unit cell is doubled in porous Si along the z axis [see Fig. 2(a)], the bulk state at the X point ($k_z = \frac{2\pi}{a}$) is folded to the Γ point and the bulk conduction-band minimum at $k_z = 0.85(\frac{2\pi}{a})$ is folded to $k_z = 0.15(\frac{2\pi}{a})$. The energies of fourfold states near the zone center increase with k_z, while the energy of the lower branch of the twofold states decreases with k_z. They cross at about $k_z = 0.11(\frac{2\pi}{a})$. For the square-wire structure there is almost no energy dispersion for $\mathbf{k}$ in the plane perpendicular to the wire, because the wires are isolated from one another.

Figure 4 shows the energy bands of the square-pore structure for $\mathbf{k}$ along the z axis. In this case, the lowest-lying conduction bands are twofold degenerate at Γ and they split as k_z increases, while the nearly fourfold degenerate bands lie at about 0.3–0.4-eV higher. Since the twofold degenerate bands are derived from X valleys along the z axis, they have different symmetry properties from those derived from the X valleys in the XY plane. Thus, we expect quite different luminescence behavior for this structure as compared to the square-wire structure.

TABLE I. Energies of conduction-band states at the Γ point for the three structures shown in Fig. 1 in the (001) and (110) porous Si. Cn and Vn denote the nth conduction and valence states, respectively. All energies are in units of eV, relative to the top of valence band of bulk Si.

	(001) Porous Si			(110) Porous Si		
Band	Case 1	Case 2	Case 3	Case 1	Case 2	Case 3
$V1$	-0.3625	-0.2492	-0.2524	-0.2178	-0.2170	-0.3090
$V2$	-0.3625	-0.2492	-0.2524	-0.2835	-0.4228	-0.4816
$V3$	-0.3767	-0.6700	-0.3810	-0.3946	-0.4511	-0.5536
$V4$	-0.4090	-0.8132	-0.4818	-0.4174	-0.4585	-0.6055
$C1$	1.3693	1.4872	1.4537	1.2201	1.2419	1.3443
$C2$	1.3805	1.4881	1.4604	1.3285	1.2621	1.5236
$C3$	1.3819	1.8003	1.4615	1.4124	1.3958	1.6624
$C4$	1.4027	1.8246	1.4829	1.5415	1.4425	1.8697

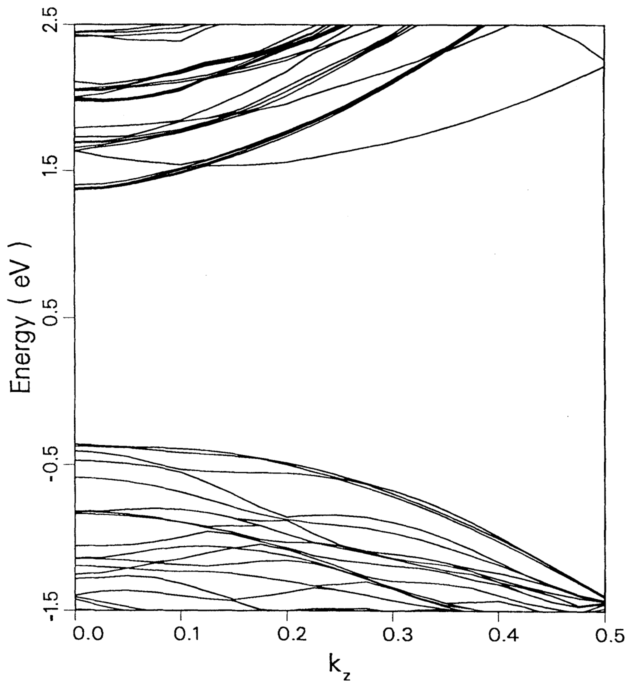

FIG. 3. Energy bands along k_z for the (001) square-wire structure. k_z is in units of $\frac{2\pi}{a}$.

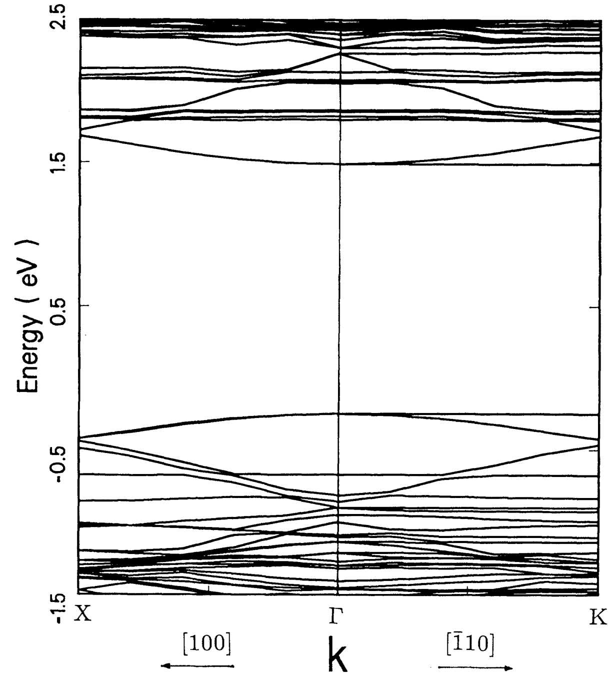

FIG. 5. Energy band along $k_{[100]}$ and $k_{[110]}$ for the (001) square-pore structure.

Figure 5 shows the energy bands of the square-pore structure for **k** along the [100] direction (from Γ to X), and along the [110] direction (from Γ to K [$\mathbf{k} = (1/2l, 1/2l, 0)\frac{2\pi}{a}$]) in the superlattice Brillouin zone [see Fig. 2(b)]. Unlike the square-wire structure both the conduction and valence bands in this case have significant dispersion along the [100] direction. Along the [110] direction both the conduction and valence bands split into two bands with one nearly dispersionless. Thus, both the electron and hole motions are nearly two dimensional.

Figure 6 shows the energy bands of the circular pore structure for **k** along the z axis. This case is intermediate

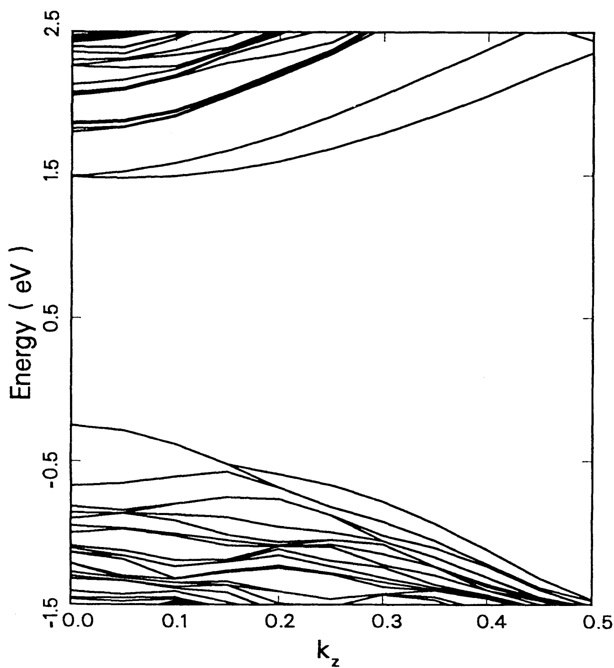

FIG. 4. Energy bands along k_z for the (001) square-pore structure. k_z is in units of $\frac{2\pi}{a}$.

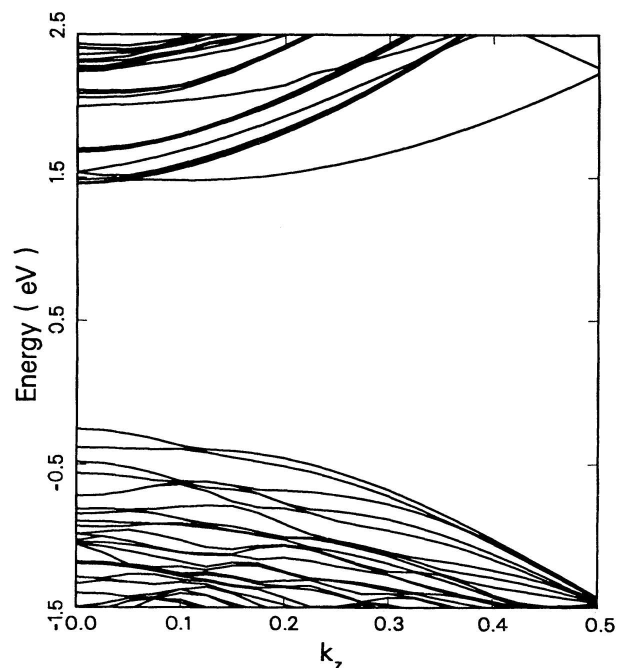

FIG. 6. Energy bands along k_z for the (001) circular-pore structure. k_z is in units of $\frac{2\pi}{a}$.

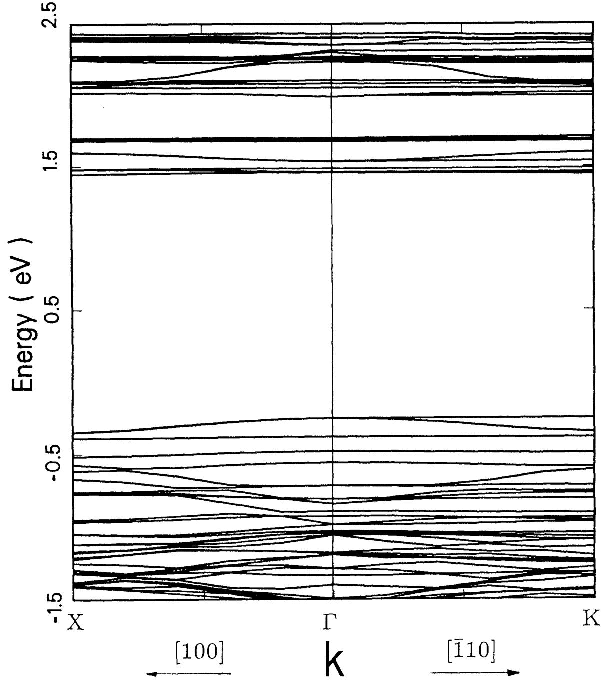

FIG. 7. Energy band along $k_{[100]}$ and $k_{[110]}$ for the (001) circular-pore structure.

between the previous two cases. The lowest-lying conduction bands are nearly fourfold degenerate, but the twofold degenerate bands lie closely above at the zone center. The energy difference between the Γ minimum and the Δ minimum in the preset structure is only about 0.02 eV. The valence-band maximum remains at the Γ point. At low temperatures the luminescence of this structure is determined mainly by states near the Γ point, while at room temperature, we expect the indirect mimimum to contribute via the phonon-assisted recombination.

Figure 7 shows the energy bands of the circular pore structure for **k** along the [100] direction (from Γ to X), and along the [110] direction (from Γ to K [$\mathbf{k} = (1/2l, 1/2l, 0)\frac{2\pi}{a}$]) in the superlattice Brillouin zone [see Fig. 2(b)]. For the conduction bands the energy dispersion for **k** in the XY plane is much smaller than that in the [001] direction. Thus, the electron motion is nearly one dimensional. The valence band, however, has appreciable dispersion along the [100] direction and it splits into two bands along the [110] direction. Thus, the hole motion is at least two dimensional.

Table II lists the optical transition matrix elements for (x, y) polarization $[\frac{1}{2}(Q^x_{nn'} + Q^y_{nn'})]$ and z polarization $(Q^z_{nn'})$ [Eq. (7)] from the four lowest conduction states to the four highest valence states at Γ for the three structures of (001) porous Si. We see that due to the quantum confinement effect there is a mixing between bulk X states and Γ states, resulting in finite optical transition matrix elements, but still much smaller than the matrix elements for direct transition between bulk Γ states. For bulk Γ'_2-Γ'_{25} and Γ_{15}-Γ'_{25} transitions, we have

$$\frac{2}{m_0}|\langle s|p_x|x'\rangle|^2 = 21.30 \text{ eV}, \quad (8)$$

$$\frac{2}{m_0}|\langle x|p_y|z'\rangle|^2 = 15.45 \text{ eV}, \quad (9)$$

where $|s\rangle$ is a conduction Γ'_2 state, $|x\rangle$ is a conduction Γ_{15} state, and $|x'\rangle$ and $|z'\rangle$ are valence Γ'_{25} states. For porous Si the transitions from the twofold conduction states involve mainly the bulk states located near the two X minima along the z axis, and those from the fourfold states involve the bulk states located near the four X minima in the XY plane. In the three cases of porous

TABLE II. Optical transition matrix elements squared $\frac{1}{2}(Q^x_{nn'} + Q^y_{nn'})$ and $Q^z_{nn'}$ (in units of eV) at the Γ point for the three structures of (001) porous Si. Cn and Vn denote the nth conduction and valence states, respectively. The last digit after the minus sign indicates the exponent, e.g., −4 means 10^{-4}.

	(x,y) polarization			z polarization		
	Case 1	Case 2	Case 3	Case 1	Case 2	Case 3
$C1$-$V1$	0.454-4	0.181-3	0.352-3	0.472-4	0.235-5	0.216-2
$C2$-$V1$	0.139-4	0.441-3	0.116-3	0.176-3	0.253-4	0.164-5
$C3$-$V1$	0.151-3	0.209-3	0.154-2	0.549-5	0.303-3	0.578-4
$C4$-$V1$	0.305-4	0.246-1	0.150-3	0.304-2	0.582-7	0.335-2
$C1$-$V2$	0.105-4	0.479-3	0.160-5	0.935-3	0.441-4	0.124-1
$C2$-$V2$	0.201-4	0.862-3	0.389-4	0.945-3	0.293-4	0.470-3
$C3$-$V2$	0.384-3	0.236-3	0.532-3	0.523-4	0.165-5	0.399-3
$C4$-$V2$	0.528-4	0.243-1	0.489-4	0.685-2	0.462-5	0.168-2
$C1$-$V3$	0.301-4	0.153-3	0.203-3	0.230-3	0.486-2	0.423-2
$C2$-$V3$	0.547-5	0.322-3	0.410-5	0.419-3	0.341-2	0.310-3
$C3$-$V3$	0.243-3	0.521-3	0.131-3	0.645-4	0.174-2	0.197-4
$C4$-$V3$	0.438-6	0.225-3	0.187-3	0.170-2	0.280-1	0.162-1
$C1$-$V4$	0.237-5	0.178-2	0.194-4	0.253-3	0.249-2	0.324-2
$C2$-$V4$	0.483-5	0.199-3	0.196-4	0.135-3	0.846-3	0.171-4
$C3$-$V4$	0.251-2	0.240-4	0.457-2	0.107-4	0.392-3	0.252-3
$C4$-$V4$	0.882-6	0.180-2	0.291-3	0.120-2	0.804-3	0.955-3

Si considered here, the structure with circular pores has the larger optical transition matrix elements for low-lying states compared to two other structures. For example, in case 3 both the $C3$-$V1$ and $C3$-$V4$ transitions are strong for (x,y) polarization and both the $C1$-$V2$ and $C4$-$V3$ transitions are very strong for z polarization. Thus, this structure may play an important role in determining the luminescence observed in porous Si for photon energies near 1.6 eV. Of course, the excitonic effect also needs to be considered. Here because of the finite dispersion for valence bands along directions in the XY plane, we expect the excitonic enhancement effect is weaker compared to that for free-standing wires (see Ref. 5). Taking into account both excitonic effects and optical matrix elements, we estimate the contributions from both structures to be comparable. For case 2 (the square pore structure), only the lowest two conduction bands and the highest two valence bands are near the band edges (see Table I); thus, although some optical transitions involving these higher bands are strong [e.g., $C4$-$V1$, $C4$-$V2$ (x,y), or $C4$-$V3$ (z)], they do not contribute to the luminscence.

In addition to (001) porous Si discussed above, we also considered (110) porous Si, i.e., with wires or pores aligned perpendicular to the (110) plane. In this case the wave functions for the porous Si are expanded by the Bloch waves with the following wave vectors $\mathbf{k}+\mathbf{g}$:

$$g_2 = \frac{2\pi}{n\frac{\sqrt{2}}{2}a} l_2, \qquad l_2 = -[(l-1)/2], \ldots, 0, \ldots, [l/2], \tag{10}$$

$$g_z = \frac{2\pi}{ma} l_3, \qquad l_3 = -[(m-1)/2], \ldots, 0, \ldots, [m/2], \tag{11}$$

$$-\frac{\sqrt{2}\pi}{a} < k_1 < \frac{\sqrt{2}\pi}{a}. \tag{12}$$

We choose a superlattice unit cell with $l = 10$ and $m = 8$, i.e., the lengths of the two edges are $10\frac{\sqrt{2}}{2}a = 38.4$ Å and $8a = 43.4$ Å in the $[\bar{1}10]$ and [001] directions, respectively. The sizes of three structures with the same geometries as shown in Fig. 1 are taken to be similar to those in (001) porous Si. In the first case, the lengths of the two edges for the rectangular wire are taken as $6\frac{\sqrt{2}}{2}a = 23$ Å and $4a=21.7$ Å, respectively; in the second case, the lengths of the two edges for the rectangular pore are taken as $8\frac{\sqrt{2}}{2}a = 30.7$ Å and $6a=32.6$ Å, respectively; and in the third case, the radius of the circular pore is taken as $4\frac{\sqrt{2}}{2}a = 15.4$ Å.

The eigenenergies of the lowest four conduction states and highest four valence states at the Γ point $[\mathbf{k}=(0,0,0)]$ for the three structures of (110) porous Si are shown in Table I. Similarly to the (001) porous Si the energy of the ground state at the Γ point is the lowest. There are some noticeable differences between the (001) porous Si and the (110) porous Si. In the (110) porous Si there are only nearly twofold or singlet states (excluding spin degeneracy). The singlet states are composed mainly of bulk states located near the [001] or $[00\bar{1}]$ X points folded to the Γ point. The bulk states located near the other four X valleys in the XY plane have no contribution to

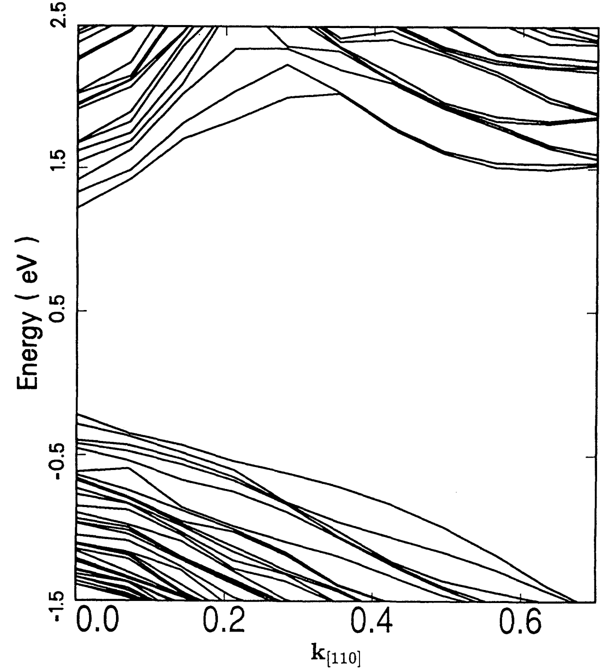

FIG. 8. Energy bands along $k_{[110]}$ for the (110) rectangular-wire structure. $k_{[110]}$ is in units of $\frac{2\pi}{a}$.

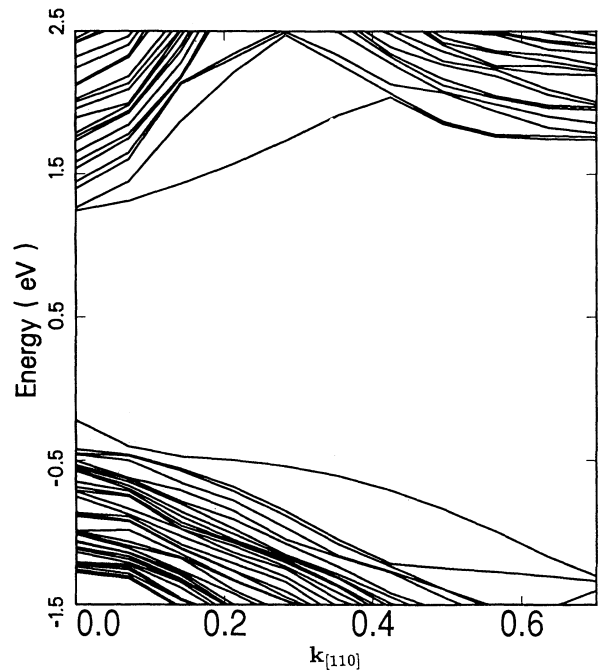

FIG. 9. Energy bands along $k_{[110]}$ for the (110) rectangular-pore structure. $k_{[110]}$ is in units of $\frac{2\pi}{a}$.

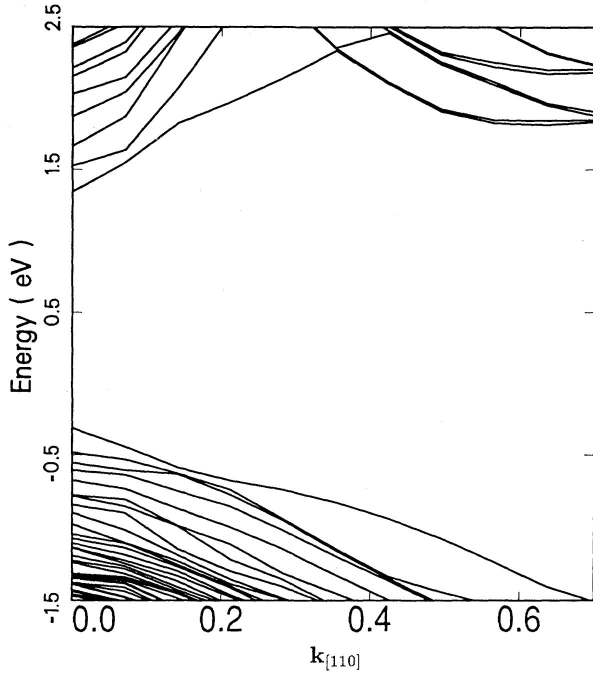

FIG. 10. Energy bands along $k_{[110]}$ for the (110) circular-pore structure. $k_{[110]}$ is in units of $\frac{2\pi}{a}$.

the conduction-band states at the Γ point, since the projection of these valleys on the [110] axis always has a finite value of $k_{[110]}$. The energies of the lowest-lying bands are considerably lower than those of the counterparts of (001) porous Si (although with a similar cross-sectional area). This is attributed to the heavy effective mass along one direction of quantization (i.e., [001]).

The energy bands of the three structures for (110) porous Si along the $k_{[110]}$ direction are shown in Figs. 8–10. From these figures we see that there are two energy local minima: one is at the Γ point, the other with nearly double degeneracy and higher energy is at $k_{[110]}=0.6(\frac{2\pi}{a})$, which is derived from bulk Δ minima states with wave vectors in the XY plane. The energy bands of the (110) porous structure with pores have a similar shape, with the conduction-band minimum also located at the Γ point. The dispersion of low-lying bands along the [001] and [$\bar{1}$10] directions are found to be rather weak for all three geometries (not shown), indicating a quasi-one-dimensional behavior.

Table III lists the optical transition matrix elements for (x,y) polarization $[\frac{1}{2}(Q^x_{nn'}+Q^y_{nn'})]$ and z polarization $(Q^z_{nn'})$ [Eq. (7)] from the four lowest conduction states to the four highest valence states at Γ for the three structures of (110) porous Si. In general, the optical matrix elements for z polarization are much stronger than those for (x,y) polarization. This is expected as the lowest conduction-band states are mainly derived from bulk Si states with wave vectors near the [001] Δ valley. In case 2 the optical matrix element for the lowest-energy transition is strong (≈ 0.011 eV), and in the other two cases we find no optical matrix elements stronger than 10^{-3} eV for transitions involving the lowest two conduction bands. Thus, we expect that the luminscence in (110) porous Si is dominated by the pore structure with the square cross section.

IV. SUMMARY

In summary, we presented a theoretical model for the electronic structure of porous Si. This model is applicable in principle to semiconductor quantum wires and porous structures with an arbitrary cross section or crystalline orientation. Due to the quantum confinement effect, there is a mixing between the bulk X and bulk Γ states, resulting in finite optical transition matrix ele-

TABLE III. Optical transition matrix elements squared $\frac{1}{2}(Q^x_{nn'}+Q^y_{nn'})$ and $Q^z_{nn'}$ (in units of eV) at the Γ point for the three structures of (110) porous Si. Cn and Vn represent conduction and valence states, respectively. The last digit after the minus sign indicates the exponent, e.g., −4 means 10^{-4}.

	(x,y) polarization			z polarization		
	Case 1	Case 2	Case 3	Case 1	Case 2	Case 3
$C1$-$V1$	0.258-6	0.406-6	0.488-5	0.968-4	0.110-1	0.157-3
$C2$-$V1$	0.297-11	0.195-7	0.291-12	0.869-3	0.281-2	0.139-3
$C3$-$V1$	0.197-4	0.704-6	0.564-5	0.327-12	0.427-2	0.856-10
$C4$-$V1$	0.120-5	0.375-4	0.514-4	0.206-2	0.496-4	0.899-4
$C1$-$V2$	0.703-5	0.111-5	0.550-4	0.896-3	0.177-2	0.857-3
$C2$-$V2$	0.424-11	0.140-6	0.617-11	0.583-4	0.676-3	0.280-2
$C3$-$V2$	0.401-4	0.561-6	0.190-4	0.509-10	0.273-3	0.117-10
$C4$-$V2$	0.169-5	0.731-4	0.429-3	0.474-3	0.280-3	0.451-3
$C1$-$V3$	0.484-6	0.453-5	0.197-4	0.169-2	0.237-3	0.165-3
$C2$-$V3$	0.192-12	0.582-5	0.313-11	0.310-2	0.250-2	0.818-2
$C3$-$V3$	0.218-4	0.385-5	0.849-4	0.524-10	0.509-3	0.826-11
$C4$-$V3$	0.543-6	0.225-2	0.197-3	0.126-1	0.137-1	0.364-3
$C1$-$V4$	0.243-4	0.815-5	0.112-3	0.481-3	0.196-2	0.963-3
$C2$-$V4$	0.760-11	0.131-4	0.683-11	0.460-3	0.880-3	0.107-1
$C3$-$V4$	0.156-3	0.587-5	0.109-4	0.273-10	0.597-2	0.121-9
$C4$-$V4$	0.187-5	0.380-2	0.615-3	0.364-3	0.158-1	0.135-2

ments, but it is smaller than the usual direct transition matrix elements by three orders of magnitude. Three geometries of porous Si along two different orientations [(001) and (110)] have been considered; it is found that the confinement geometry affects decisively the energies and ordering of conduction-band states. For the (001) porous Si the structure with circular pores has larger optical transition matrix elements compared to two other structures and it should be considered in understanding the observed luminescence. The energy difference between the direct and indirect conduction minima in this structure is very small. When the phonon-assisted recombination is considered these indirect minima may also play an important role in the luminescence. In fact, phonon-assisted recombination may be important even for the direct transitions, since the electron-phonon coupling can mix the Γ- and X-derived states and lead to enhanced optical matrix elements. The relative strength for the phonon-assisted transition as compared to the dipole-allowed transition induced by quantum confinment effects would be an important issue to study. For the (110) porous Si we found that the optical transition matrix elements are of the same order of magnitude as in the (001) case, but they are more anisotropic with the z polarization dominating the x, y polarization. For a similar size of cross section, the (110) porous Si tends to have a smaller band gap compared to (001) porous Si.

ACKNOWLEDGMENTS

This work was supported in part by the U.S. Office of Naval Research (ONR) under Contract No. N00014-89-J-1157. The use of the computing facilities of the University of Illinois Materials Research Laboratory is acknowledged.

---

*Permanent address: National Laboratory for Superlattices and Microstructures, Institute of Semiconductors, Chinese Academy of Sciences, P.O. Box 912, Beijing 100083, China.

[1] L.T. Canham, Appl. Phys. Lett. **57**, 1046 (1990).

[2] A. Halimaoui, C. Oules, G. Bomchil, A. Bsiesy, F. Gaspard, R. Herinop, M. Liggeon, and F. Muller, Appl. Phys. Lett. **59**, 304 (1991).

[3] L.T. Canham, M.R. Houlton, W.Y. Leong, C. Pickering, and J.M. Keen, J. Appl. Phys. **70**, 422 (1991).

[4] R. Tsu, H. Shen, and M. Dutta, Appl. Phys. Lett. **60**, 112 (1992).

[5] G.D. Sanders and Y.C. Chang, Phys. Rev. B **45**, 9202 (1992).

[6] T. Ohno, K. Shiraishi, and T. Ogawa, Phys. Rev. Lett. **69**, 2400 (1992).

[7] C. Pickering, M.I.J. Beale, D.J. Robbins, P.J. Pearson, and R. Greef, J. Phys. C **17**, 6535 (1984).

[8] R.P. Vasquez, R.W. Fathauer, T. George, A. Ksendzov, and T.L. Lin, Appl. Phys. Lett. **60**, 1004 (1992).

[9] X.L. Zheng, W. Wang, and H.C. Chen, Appl. Phys. Lett. **60**, 986 (1992).

[10] M.S. Brandt, H.D. Fuchs, M. Stutzmann, J. Weber, and M. Cardona, Solid State Commun. **81**, 307 (1992).

[11] M.L. Cohen and T.K. Bergstresser, Phys. Rev. **141**, 789 (1966).

[12] M.L. Cohen and V. Heine, in *Solid State Physics*, edited by F. Seitz, D. Turnbull, and H. Ehrenreich (Academic, New York, 1968), Vol. 24, p. 38.

[13] J.B. Xia and A. Baldereschi, Chinese J. Semicond. **8**, 584 (1987); Chinese Phys. **8**, 1074 (1988).

[14] J.B. Xia, Phys. Rev. B **38**, 8358 (1988).

[15] M. Schlüter, J.R. Chelikowsky, S.G. Louie, and M.L. Cohen, Phys. Rev. B **12**, 4200 (1975).